Anteroposterior Hippocampal Metabolic Heterogeneity: Three-dimensional Multivoxel Proton ^{1}H MR Spectroscopic Imaging—Initial Findings[1]

Kevin G. King, MD
Lidia Glodzik, MD, PhD
Songtao Liu, MD
James S. Babb, PhD
Mony J. de Leon, EdD
Oded Gonen, PhD

Purpose: To quantify proton magnetic resonance (MR) spectroscopy–detectable metabolite concentrations along anteroposterior axis of hippocampus in healthy young and elderly subjects.

Materials and Methods: Young (three women, three men; age range, 25–35 years) and elderly (four women, two men; age range, 68–72 years) groups underwent MR imaging and proton MR spectroscopic imaging at 3 T in this HIPAA-compliant prospective study and gave institutional review board–approved written consent. Volume of interest was centered on and tilted parallel to hippocampal anteroposterior plane. Absolute *N*-acetylaspartate (NAA), choline, and creatine levels were obtained in each voxel, with phantom replacement.

Results: Mean NAA, creatine, and choline concentrations in the young group were higher in posterior hippocampus (12.9 mmol/L ± 2.0 [standard deviation], 7.8 mmol/L ± 1.2, 2.3 mmol/L ± 0.4, respectively) than anterior hippocampus (8.0 mmol/L ± 1.1, 6.0 mmol/L ± 1.4, 1.5 mmol/L ± 0.2; P = .005, .02, and .0002, respectively). In the elderly group, mean concentrations were higher in posterior hippocampus (8.6 mmol/L ± 0.9, 5.6 mmol/L ± 0.6, 1.5 mmol/L ± 0.2, respectively) than anterior hippocampus (7.2 mmol/L ± 1.0, 2.4 mmol/L ± 0.3, 1.0 mmol/L ± 0.2; P = .006, .0001, .04, respectively). Mean concentrations were significantly higher in the young group (13.2 mmol/L ± 1.0, 7.4 mmol/L ± 0.8, 2.1 mmol/L ± 0.3, respectively) than in the elderly group (9.0 mmol/L ± 1.0, 5.8 mmol/L ± 0.8, 1.8 mmol/L ± 0.3; P = .0001, .01, .05, respectively). Posteroanterior metabolic gradients differed: NAA decreased faster in the young group (−1.0 mmol/L · cm^{-1}) than the elderly group (−0.7 mmol/L · cm^{-1}); creatine and choline concentrations decreased faster in the elderly group (−0.8 and −0.058 mmol/L · cm^{-1}, respectively) than the young group (−0.16 and −0.008 mmol/L · cm^{-1}, respectively). No left-right metabolic differences were found.

Conclusion: Significant metabolic heterogeneity was observed between groups and along anteroposterior axis of healthy hippocampus in both groups. Age matching and consistent voxel placement are important for correct comparisons of both absolute metabolic levels and metabolite ratios in longitudinal intra- and intersubject cross-sectional studies.

[1] From the Departments of Radiology (K.G.K., S.L., J.S.B., O.G.) and Psychiatry (L.G., M.J.d.L.), Center for Brain Health, New York University School of Medicine, 550 First Ave, New York, NY 10016. Received August 23, 2007; revision requested November 13; revision received January 8, 2008; accepted March 11; final version accepted April 17. Supported by National Institutes of Health grants EB01015, NS050520, AG12101, AG08051, AG03051 and RR0096. K.G.K. supported by grant NCRR M01RR00096 from the Mentored Medical Student Clinical Research Program. **Address correspondence to** O.G. (e-mail: *oded.gonen@med.nyu.edu*).

The hippocampus, a part of the limbic system located on the floor of the temporal horn of the lateral ventricle (1), is crucial for memory consolidation, spatial cognition, perception of temporal ordering of events (2), mood regulation (3), and negative feedback inhibition of glucocorticoids (4). It is functionally connected to a wide range of cortical and subcortical brain regions, including the cingulate gyrus, orbitofrontal and temporal cortices, amygdala, olfactory cortex, and thalamic nuclei (5). Given this complex function and connectivity, it is not surprising that abnormalities of the hippocampus play a major role in many prevalent neurologic disorders (eg, Alzheimer disease [1], epilepsy [6], major depression [3], schizophrenia [7], and posttraumatic stress disorder [8]).

Magnetic resonance (MR) imaging for structural and functional assessment and proton hydrogen 1 (^{1}H) MR spectroscopy for metabolic and physiologic assessment both are often used for noninvasive studies of the hippocampus (9). ^{1}H MR spectroscopic measurements can serve as estimates of neuronal cell viability, cell energetics, membrane turnover, gliosis, glycolysis, and inflammatory processes in vivo through levels of their respective surrogate markers, *N*-acetylaspartate (NAA), creatine, choline, *myo*-inositol, and lactate (10–12). Furthermore, because ^{1}H MR spectroscopy has shown variable changes among brain regions (13,14), its three-dimensional MR spectroscopic imaging variant is of great utility in the evaluation of an increasing number of clinical conditions. MR spectroscopic imaging improves diagnostic accuracy for differentiation between recurrent neoplastic brain lesions and therapy-related effects (15), for preoperative assignment of grades to gliomas (16), and for localization of an epileptogenic focus in the medial temporal lobe (17).

^{1}H MR spectroscopic imaging already has revealed hippocampal metabolic differences between patients and control subjects in the assessment of a variety of brain disorders. In Alzheimer disease, for example, two findings are consistent: a decrease in NAA, representing neuronal atrophy or dysfunction, and an increase in *myo*-inositol, reflecting gliosis (18). Similarly, in medial temporal lobe epilepsy, ^{1}H MR spectroscopy showed ipsilateral hippocampal NAA decreases with sufficient sensitivity to lateralize epileptogenic foci (19,20).

It is clear, then, that the clinical uses of ^{1}H MR spectroscopy in the examination of the hippocampus are numerous and substantial, and, therefore, it is all the more important to characterize the normal metabolic distribution of this structure. There are histoanatomic reasons to suspect nonuniformity: First, the hippocampus comprises a mixture of gray matter and white matter. Its gray matter is composed of two interlocking cortical lamina, the dentate gyrus and the cornu ammonis (hippocampus proper). White matter axons in the alveus and fimbria not only ensheathe the hippocampus but also are interposed between its gray matter laminae. Second, the hippocampus is not histologically uniform, with an increase in the density of pyramidal cells and a decrease in the density of granular cells along its anteroposterior axis (21,22).

Some spectroscopic heterogeneity already has been observed: A posterior-to-anterior decrease in the NAA/(creatine + choline) ratio along the hippocampus was seen in patients with medial temporal lobe epilepsy (bilaterally) and young control subjects (23). An NAA/creatine ratio decrease in control subjects and medial temporal lobe epilepsy (ipsilateral only) patients was reported but not specifically discussed by Hetherington et al (24). Because the hippocampus is increasingly the focus of clinical studies in the young and the elderly, our goal was to quantify, with high-spatial-resolution three-dimensional ^{1}H MR spectroscopy, the anteroposterior metabolic profile of the hippocampus in both age groups.

Advances in Knowledge

- The regional MR spectroscopy–detectable metabolic concentrations in the healthy human hippocampus are higher in young than in elderly neurologically healthy subjects.
- The concentrations of these metabolites vary linearly along the hippocampus axis from their highest at the posterior hippocampus to their lowest at the anterior hippocampus.
- These anteroposterior metabolite concentration gradients are age dependent and differ significantly between young adults and the elderly.

Implications for Patient Care

- The findings from this study indicate that there are significant metabolic level differences between these two age groups and among the different regions in their hippocampi.
- Clinical use of metabolic levels requires both age-matched control subjects and comparisons of analogous regions in the hippocampus between patients and control subjects.

Materials and Methods

Subjects

Twelve healthy control subjects (five men, seven women; mean age, 49.8 years; range, 25–72 years) were re-

Published online before print
10.1148/radiol.2491071500

Radiology 2008; 249:242–250

Abbreviations:
NAA = *N*-acetylaspartate
VOI = volume of interest

Author contributions:
Guarantor of integrity of entire study, O.G.; study concepts/study design or data acquisition or data analysis/interpretation, all authors; manuscript drafting or manuscript revision for important intellectual content, all authors; approval of final version of submitted manuscript, all authors; literature research, all authors; clinical studies, L.G., M.J.d.L., O.G.; experimental studies, L.G., O.G.; statistical analysis, K.G.K., S.L., J.S.B.; and manuscript editing, all authors

Funding:
This research supported by the National Institutes of Health (grants EB01015, NS050520, AG12101, AG08051, AG03051, RR0096) and National Center for Research Resources Mentored Medical Student Clinical Research Program (grant M01RR00096).

Authors stated no financial relationship to disclose.

cruited in this prospective study. Six were in the young group (three men, three women; mean age, 29.3 years; range, 25–35 years) and six were in the elderly group (two men, four women; mean age, 70.3 years; range, 68–72 years). Healthy status in the elderly was established on the basis of a Mini-Mental State Examination for general cognitive performance (25), the Global Deterioration Scale to exclude cognition-related functional issues (26), the Brief Cognitive Rating Scale interview for memory performance and global functioning (27), and a physical examination with screening MR imaging and blood chemistry analysis for general medical conditions. All gave negative answers to questions about whether they had any MR imaging contraindications or any of the 20 disqualifying neurologic conditions before imaging. MR imaging did not reveal any abnormalities. All participants gave written institutional review board–approved informed consent, and this study was Health Insurance Portability and Accountability Act compliant.

MR Imaging and Three-dimensional ^{1}H MR Spectroscopy

All MR images and ^{1}H MR spectroscopic images were obtained with a 3-T imager (Trio; Siemens Medical Solutions, Erlangen, Germany) by using a transmit-receive head coil (TEM3000; MR Instruments, Minneapolis, Minn). The supine subjects were placed head first in the imager such that an axial plane passing just below their eyes was the center of the coil and of the magnet to ensure that the hippocampi would be optimally placed for best radiofrequency (constant radiofrequency field [B_1]) and static field homogeneity. Contiguous axial, sagittal, and coronal T1-weighted spin-echo MR images (repetition time msec/echo time msec, 600/7.3; field of view, 240 × 240 mm^2; matrix, 512 × 512; and section thickness, 5 mm) were obtained.

A volume of interest (VOI) (9 × 7 × 2 cm [left-right by anteroposterior by inferosuperior directions] = 126 cm^3) was positioned with image guidance to parallel the hippocampal axis, as shown in Figure 1. Our three-dimensional chemical shift imaging–based shimming produced a consistent mean 19 Hz ± 4 (standard deviation) VOI water resonance full width at half maximum line width (28).

The VOI was selectively excited with point-resolved spatially localized spectroscopy (1600/39), and the VOI was divided into four sections with fourth-order Hadamard encoding for optimal sensitivity (29). These sections were subdivided with 16 × 16 two-dimensional MR spectroscopic imaging in the left-right by anteroposterior planes (field of view, 16 × 16 cm^2), leading to 1.0 × 1.0 × 0.5 = 0.5 cm^3 nominal spatial resolution (or approximately 1.12 × 1.12 × 0.5 = 0.63 cm^3, considering the full width at half maximum of the point-spread function for the uniform two-dimensional phase encoding [30, 31]), as shown in Figure 1. The signals were acquired with 1024 complex points for 512 msec, for a 2-Hz per-point resolution. Two signals were acquired in 27 minutes, and the entire protocol was performed in less than 1 hour.

The signal-to-noise ratio and spectral resolution achieved in this 27-minute acquisition can be appreciated in the axial spectra matrix shown in Figure 2, top. In Figure 2, middle, sample voxels are expanded for detail over the 0–3.7-ppm chemical shift range for better visualization of the noise in the higher field region. The raw spectra, the fitted spectra, and the fitted spectra subtracted from the raw spectra are shown; note the signal-to-noise ratio, resolution, and quality of the fit. Axial metabolic maps (Fig 2, bottom) were obtained from the matrices of fitted spectra. Excellent correspondence was observed between the metabolic images and the morphology of the image above, again reflecting the overall quality of the spectra and the localization.

The maximal chemical shift displacement error in the Hadamard (inferosuperior) direction between the choline and NAA peaks, which were 150 Hz apart at 3 T, with 12 mT/m (5.1 kHz/cm) was 0.03 cm, or approximately 6% of the 0.5-cm thick MR spectroscopic image sections. The two 11.8-msec point-resolved spatially localized spectroscopic images (180° pulses) applied in the left-right and anteroposterior directions with 1.06 and 1.37 mT/m had 0.3- and 0.25-cm relative shift between the NAA and choline VOIs, respectively, in these directions. Because this shift affects only voxels at the edges of the VOI (well beyond both hippocampi boundaries, as shown in Figs 1 and 2), and the chemical shift imaging–encoded spectra within this matrix are not affected by such displacement errors (32), these shifts did not affect our results.

For the purpose of volumetric analysis, contiguous sagittal T1-weighted spin-echo MR images (2000/2.8; field of view,

Figure 1

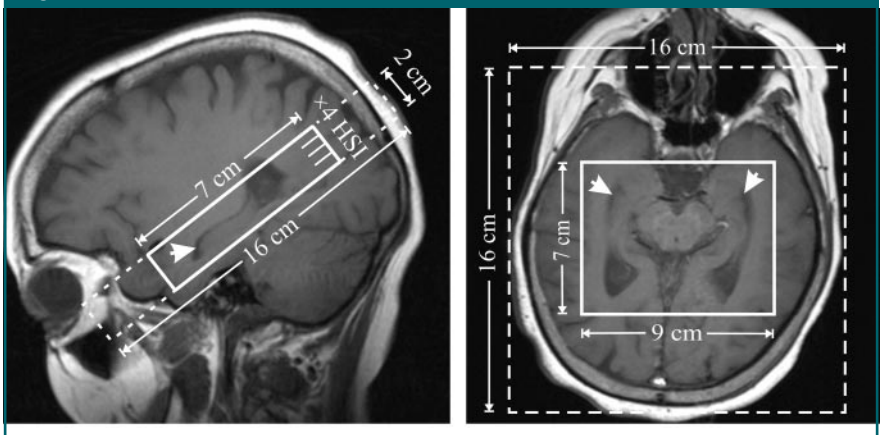

Figure 1: **(a)** Sagittal and **(b)** paraxial T1-weighted MR images (600/7.3) in healthy elderly subject shows position of field of view (dashed line) and VOI (solid line) centered on hippocampi (arrows).

240 × 240 mm^2; three-dimensional matrix, 192 × 256 × 256; and section thickness, 0.9 mm) were also obtained. Hippocampal volumetric sampling was performed by using our in-house multimodal image data analysis system software. Sagittal images were reformatted to coronal images angled perpendicular to the long hippocampal axis (sinc interpolation; section thickness, 1.5 mm). The hippocampus was manually traced on each image, starting anteriorly from the level of the anteriormost amygdala and posteriorly to the level of the posterior pulvinar (33).

Metabolite Postprocessing and Quantification

The ^{1}H MR spectroscopic data were postprocessed off-line with our in-house software by an operator with 1 year of experience (K.G.K.) supervised by a spectroscopist with more than 25 years of experience (O.G.). Neither was blinded to the nature of the data (young group vs elderly group), and no assessment of intraobserver variability was performed. The software removed residual water signals in the time domain, apodized with a 4-Hz Lorentzian filter, zero-filled from 1024 to 2048 points and spatially from 16 × 16 to 32 × 32 matrix in the left-right by anteroposterior planes, and voxel shifted to align the MR spectroscopic imaging grid with the NAA VOI. It was followed by Fourier transforms along the left-right direction, the anteroposterior direction, and time, as well as a fourth-order Hadamard transform along the inferosuperior direction (29,31). Automatic frequency and zero-order phase corrections were made in each voxel in reference to its NAA peak.

Relative NAA, creatine, and choline levels were estimated from their peak areas by using the parametric spectral model and least-squares optimization of Soher et al (34), and NAA, choline, creatine, glutamate, glutamine, taurine, and *myo*-inositol were included in the model, as shown in Figure 2. This model also accounts for different metabolite line widths among voxels that may arise from magnetic field inhomogeneities caused by regional susceptibility gradients around the hippocampus. Previous analysis of this baseline model showed that, for spectra with a 5-Hz line width, the mean errors of the fit are 3.4%, 2.3%, and 2.8% for NAA, creatine, and choline, respectively (35).

For acquiring relative peak areas, voxels were assigned to the hippocampus on the axial projection, as shown in Figure 2, and were assigned only when their grid position was entirely within that structure. The voxels were assigned on a voxel-by-voxel basis. The relative peak area of a given signal in each voxel in vivo, A_{viv}, was scaled into an absolute concentration, Q_{viv}, by using phantom replacement, with a concentration in the phantom of Q_{vit}, by repeating the same experiment on a 2-L sphere of Q_{vit} = 12.5 mmol/L NAA, 10.0 mmol/L creatine hydrate, and 3.0 mmol/L choline chloride in lightly doped water. This is seen in Figure 3, which shows an axial image from the 2-L phantom used as quantification reference overlaid with the MR spectroscopic imaging grid from one of the four sections and its corresponding measured and fitted spectra, together with the NAA, creatine, and choline metabolic maps derived from them. From Figure 3, top left

Figure 2

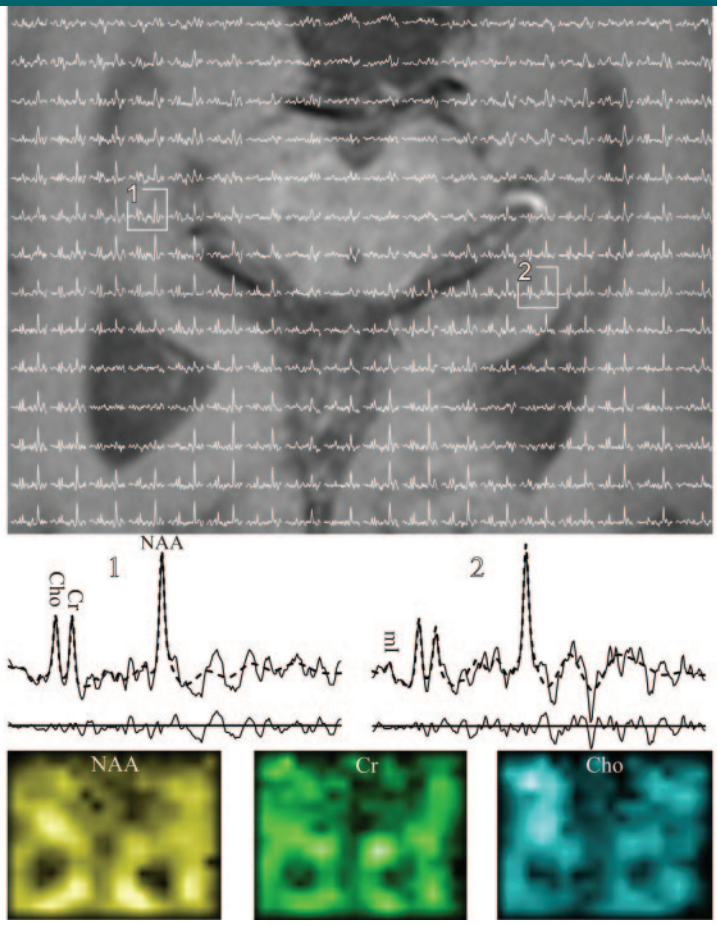

Figure 2: Top: Real part of 18 × 14 (left-right by anteroposterior directions) axial matrix of ^{1}H spectra in VOI in Figure 1b. Spectra represent 0.16-cm^3 voxels, and all share same 1.6–3.7-ppm and intensity scales. Middle: Sample voxels *1* and *2* from right and left hippocampi, respectively, in matrix above are expanded for detail over 0–3.7-ppm chemical shift range for choline *(Cho)*, creatine *(Cr)*, NAA, and *myo*-inositol *(ml)*. Upper spectra: Baseline-estimate–corrected raw spectra (solid curve) overlaid with metabolite-fitted function (dashed curve). Lower spectra: Fitted spectra and spectra of baseline estimate subtracted from residual raw spectra. Bottom: Axial metabolic maps of NAA, creatine, and choline obtained from above spectra.

and top right, relative "flatness" of both the MR image and the metabolic maps is observed, indicating good B_1 homogeneity over the phantom and especially the VOI. On Figure 3, bottom, the signal-to-noise ratio and spectral resolution, as well as the quality of the results of fitting the spectra with the spectral modeling software (SITools-FITT; Andrew A. Maudsley, PhD, University of Miami, Miami, Fla, and Brian J. Soher, PhD, Duke University, Durham, NC) and expected similar spectra in every voxel in the VOI of this homogeneous phantom, were observed.

Accounting for the different radiofrequency voltages needed for an effective 180° flip angle with the same rectangular pulse for a subject and the phantom, V_{viv} and V_{vit}, respectively, the absolute concentration (36) can be calculated with Equation (1) thus:

$$Q_{viv} = A_{vivc}\frac{Q_{vit}}{A_{vit}}\cdot\frac{V_{viv}}{V_{vit}}, \qquad (1)$$

where A_{vit} is the peak area of a metabolite in the phantom and A_{vivc} is that peak area in a subject corrected for differences in T1 and T2 relaxation times for in vivo ($T1_{viv}$ and $T2_{viv}$) versus phantom ($T1_{vit}$ and $T2_{vit}$), respectively (36), which can be calculated with Equation (2) as follows:

$$A_{vivc} = A_{viv}\frac{\exp(-TE/T2_{vit})}{\exp(-TE/T2_{viv})}\cdot\frac{1-\exp(TR/T1_{vit})}{1-\exp(TR/T1_{viv})}, \qquad (2)$$

where TE is echo time and TR is repetition time.

Values for $T1_{viv}$ are 1.4, 1.2, and 1.3 seconds and for $T2_{viv}$ are 258, 152, and 203 msec for NAA, creatine, and choline, respectively, and are the in vivo values at 3 T from the literature (37–39). Values for $T1_{vit}$ are 940, 460, and 240 msec and for $T2_{vit}$ are 483, 288, and 200 msec for NAA, creatine, and choline, respectively, and are the values measured in our phantom by using the recent two-point method optimized for precision-per-unit time of Fleysher et al (40,41). It is noted that our calculated value for T1 in vitro for choline is much shorter than the reported in vivo value. This shorter T1 value possibly may be caused by certain attributes of the phantom: Perhaps the disparate T1 value we report may be caused by light gadolinium doping, and another possibility for the disparate T1 value is that the entire choline peak in the phantom is made up of its chloride salt.

Figure 3

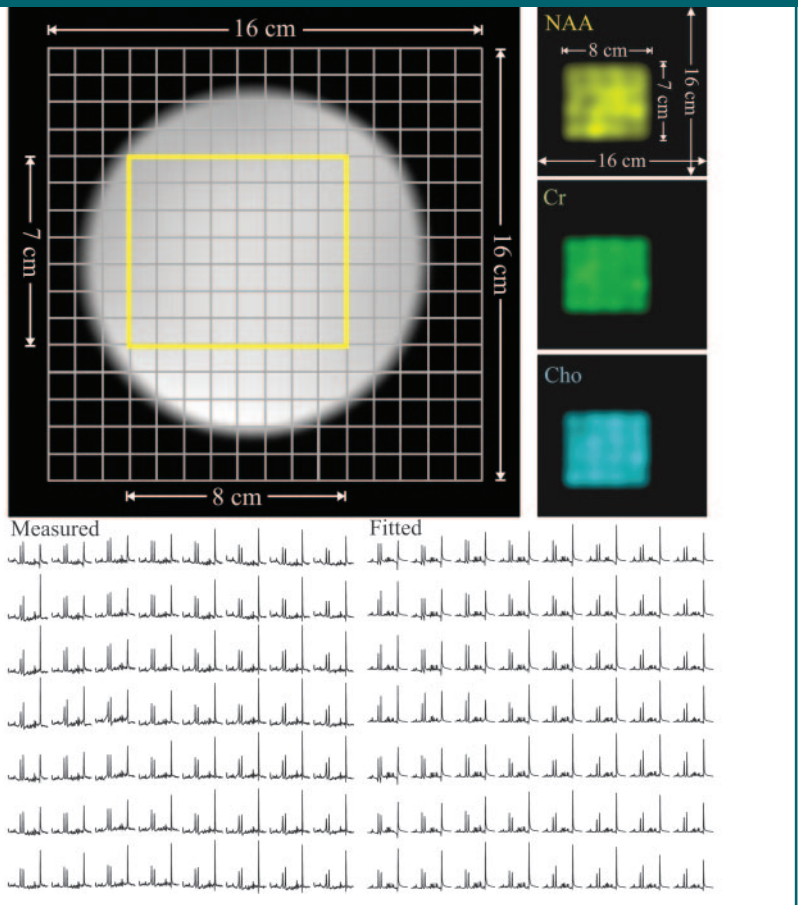

Figure 3: Top left: Axial MR image of phantom used for absolute quantification, superimposed with field of view (gray lines) and VOI (yellow box). Top right: NAA, creatine *(Cr)*, and choline *(Cho)* metabolic maps from VOI, derived from spectra in bottom. Bottom: Real part of 8 × 7 (left-right by anteroposterior directions) axial ^{1}H spectra matrix measured (left) and fitted by using spectral modeling software (right) from VOI. Spectra represent 0.63-cm^3 voxels and all share same parts-per-million and intensity scales.

Statistical Analysis

Mixed-model regression was used to examine differences across regions and between age groups with respect to choline, creatine, and NAA. A separate analysis was conducted for each metabolite, with the metabolite levels observed for all subjects in all regions of the hippocampus used as the dependent variable. The full regression model included the region, side of the measurement, sex of the subject, and age group as classification factors, along with terms representing interactions among these factors. The covariance structure was modeled by assuming observations to be correlated only when derived for the same subject and by allowing the error variance to differ across regions and age groups. When we examined whether the regional differences were different for young subjects than they were for elderly subjects, a significant region-by–age group interaction was found. This led to a separate analysis of

the young and elderly groups with respect to the differences in metabolite levels between regions. The regions were equally spaced along the anteroposterior axis of the hippocampus, so polynomial regression models could be used to assess whether the metabolites exhibited linear or quadratic changes as they progressed along this axis. All reported *P* values are two-sided and have type 3 significance level (ie, *P* values to assess the effect of one factor adjusted for the effects of all other factors included in the same model), with multiple comparison correction. A difference with a *P* value of less than .05 was significant. All statistical computations were performed by using software (SAS, version 9.0; SAS Institute, Cary, NC).

Figure 4

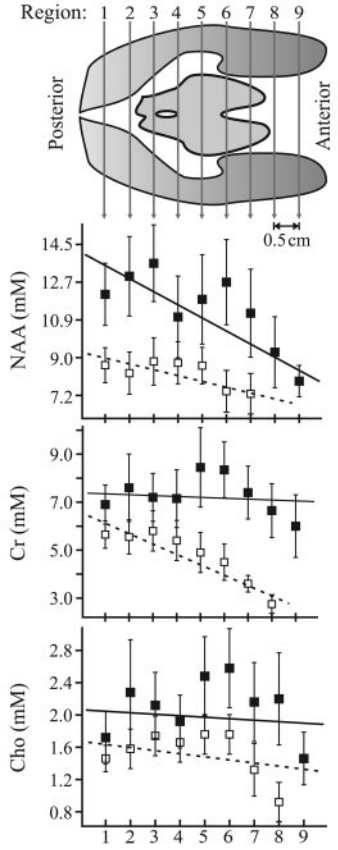

Figure 4: Top: Schematic of medial temporal lobes superimposed with anteroposterior ^{1}H MR spectroscopic localization grid regional partitions (0.5 cm apart). Bottom: Plots of means (■) and standard errors of the means (bars) of NAA, creatine *(Cr)*, and choline *(Cho)* concentrations versus hippocampal region, corresponding to schematic in top in young ($n = 6$) (■) and elderly ($n = 6$) (□). Solid (young) and dashed (elderly) lines are linear regressions of absolute metabolite concentrations versus hippocampus regions. *mM* = millimoles per liter.

Results

The mean NAA, creatine, and choline concentrations for the young ($n = 6$) and elderly ($n = 6$) groups and the standard error of the mean in each hippocampus region along the anteroposterior axis at 0.5-cm steps are shown in Figure 4. For the metabolites, there was no significant interaction ($P > .2$) between the side of the measurement (left vs right) and either age group or hippocampus region. This suggests that differences between age groups or among regions do not depend on which side of the hippocampus the metabolite measurements were performed. Consequently, metabolite concentrations are reported as averages of the concentrations for both sides.

There was a significant interaction ($P < .046$) between region and age group in terms of their effect on each metabolite, but there was no significant interaction ($P > .3$) between age group and sex. These interactions imply that regional differences are not the same among young subjects as they are among elderly subjects and that differences between age groups vary across regions of the hippocampus but do not depend on sex. Consequently, analyses to assess regional variation were stratified according to age group, and comparisons between age groups were stratified according to region but not according to sex.

The mean NAA, creatine, and choline concentrations in the young group were higher in the posterior hippocampus (12.9 mmol/L ± 2.0, 7.8 mmol/L ± 1.2, and 2.3 mmol/L ± 0.4, respectively) than in the anterior hippocampus (8.0 mmol/L ± 1.1, 6.0 mmol/L ± 1.4, and 1.5 mmol/L ± 0.2, respectively), with $P = .005$, .02, and .0002, respectively. In the elderly group, respective mean metabolite concentrations were also higher in the posterior hippocampus (8.6 mmol/L ± 0.9, 5.6 mmol/L ± 0.6, and 1.5 mmol/L ± 0.2, respectively) than in the anterior hippocampus (7.2 mmol/L ± 1.0, 2.4 mmol/L ± 0.3, and 1.0 mmol/L ± 0.2, respectively), with $P = .006$, .0001, and .04, respectively. Mean NAA, creatine, and choline concentrations were also significantly higher in the young (13.2 mmol/L ± 1.0, 7.4 mmol/L ± 0.8, and 2.1 mmol/L ± 0.3, respectively) than in the elderly (9.0 mmol/L ± 1.0, 5.8 mmol/L ± 0.8, and 1.8 mmol/L ± 0.3, respectively), with $P = .0001$, .01, and .05, respectively. As shown in Figure 4, the elderly subjects have lower concentrations of all three metabolites in all the regions. After correcting for multiple comparisons, NAA remained significantly different in regions 1–3 and 6, creatine was significantly different in regions 3–8, and choline was significantly different in regions 5–7.

For all metabolites and both age groups, linear regressions show a posterior-to-anterior decline in concentration along the hippocampus (Fig 4). These gradients differed between age groups ($P < .05$): In the young, they were -1.0 mmol/L · cm^{-1}, -0.16 mmol/L · cm^{-1}, and -0.008 mmol/L · cm^{-1} for NAA, creatine, and choline, respectively, whereas in the elderly they were -0.7 mmol/L · cm^{-1}, -0.8 mmol/L · cm^{-1}, and -0.058 mmol/L · cm^{-1}, respectively. The NAA decline was steeper in the young versus the elderly, but the reverse was true for creatine and choline, with the decline steeper in the elderly than in the young.

Polynomial regressions were also tested to see whether nonlinear fits better represented the data (ie, whether a higher concentration of any metabolite occurred away from the edges). Among the elderly, there was a significant quadratic component ($P < .05$) for the choline concentration across the hippocampus. For creatine, there was a trend toward quadratic behavior for both the young ($P < .1$) and the elderly ($P < .1$). No age group had significant quadratic behavior in the NAA component.

The uniformity of the MR images and MR spectroscopic images, evi-

denced by the homogeneity of the phantom spectra and metabolic maps, reflects the relatively minor radiofrequency field inhomogeneity across the VOI. Specifically, although the concentration of each metabolite should be the same in every voxel of this phantom, the mean concentrations were estimated to be 12.5 mmol/L ± 1.8, 10.0 mmol/L ± 1.5, and 3.0 mmol/L ± 0.4 for NAA, creatine, and choline, respectively. These nonzero standard deviations comprise all components of the variances, including those from B_1 inhomogeneities, which are, therefore, responsible for less than 15%. The mean voxel line widths of the spectra in Figure 3 are estimated to be 4.0 Hz ± 0.2, or no more than ± 5%, leading to projected mean metabolite level estimate errors of 3.4%, 2.3%, and 2.8% for NAA, creatine, and choline, respectively (35).

For volumetry, hippocampi were sampled on reformatted coronal projections and volumes are given as the percentage of total intracranial volume (33). The mean volume of the right hippocampus in the elderly group was 0.25% ± 0.03, whereas in the young group it was 0.25% ± 0.01, with a mean difference of 0% (t = 0.45, df = 9, P = .88). The mean volume of the left hippocampus in the elderly group was 0.22% ± 0.04, whereas in the young group it was 0.24% ± 0.01, with a mean difference of 9% (t = −1.23, df = 9, P = .25).

Discussion

We demonstrated that there is a heterogeneous distribution of metabolites within the hippocampus and that, in general, there is a higher concentration of metabolites posteriorly than anteriorly. In addition, we found that concentrations are higher for the young than for the elderly everywhere along the hippocampus. These findings are consistent with data in previous reports about this structure (42) and other brain regions (43–45). Specifically, the levels of NAA, creatine, and choline are higher at the posterior hippocampus, findings that are consistent with those in the study by Vermathen et al (23) who reported a decreasing NAA/(creatine + choline) ratio along that axis. We also note, however, that there is some weaker evidence that the level of some metabolites may follow a more complex distribution along the hippocampus (ie, with the highest concentration neither anterior nor posterior but somewhere between the two). For choline in the elderly, this evidence was significant ($P < .05$), but for creatine in both age groups there was only a trend toward such a distribution ($P < .1$).

It is likely that differences in the function and connectivity of the anterior versus the posterior of the hippocampus underlie the observed metabolic heterogeneity along this axis. Indeed, electrophysiologic studies seem to indicate a difference in function between the two regions, with the posterior hippocampus involved in encoding of visuospatial memory to a much greater degree than the anterior hippocampus. Indeed, in vivo electrophysiologic studies with microelectrodes in monkeys (46) and humans (47) showed greater activation (in response to a spatial task or a visual stimulus, respectively) in the posterior hippocampus than in the anterior hippocampus. Electrophysiologic studies have also borne out that there is a higher density of "place" cells in the posterior portion than in the anterior portion; these cells are thought to map out spatial correlates within the hippocampus (48).

Besides the functional distinction between the two parts of the hippocampus, there is a difference in their connectivity, which is probably related to that distinction, with the rest of the brain. Specifically, the anterior portion has strong efferent connections with the rostral hypothalamus and amygdala, connections not seen with the posterior portion (49). The posterior portion has projections to the mammillary complex, but most of its connections are afferents coming from the visual, auditory, and somatosensory cortices (50). The two parts also project to different sections of the lateral septal nuclei (51).

It is reasonable to link the differences in function and connectivity discussed previously with the metabolic level heterogeneity observed. The differences in function and connectivity could be related to the known histologic differences in cell types between the anterior hippocampus and posterior hippocampus. These, in turn, could reflect subtle but significant differences between the two regions in neuronal density (NAA), cell energetics (creatine), and membrane density (choline). Finally, possible methodological reasons for apparent lower concentrations in the anterior hippocampus cannot be ignored (eg, field inhomogeneity broadening that biases quantification).

Besides the anteroposterior metabolic heterogeneity, the concentrations of NAA, creatine, and choline were significantly higher in the young than in the elderly in many regions of the hippocampus. Although this finding could be ascribed to age-related atrophy, both groups comprised healthy individuals and, therefore, substantial atrophy is unlikely. The lack of significant differences in hippocampal volumes also argues against this possibility. Although some reports substantiate age-related reduction in NAA, creatine, and choline levels in various brain regions (43–45), others indicate stable metabolite levels (52–54). The results concerning the hippocampus are also not consistent. Some argue that the decrease in NAA is a disease-related but not age-related phenomenon, which was corroborated by a significant frontal but not hippocampal NAA decline (55). However, in line with our results, findings in a number of studies indicate age-related metabolite reductions in this structure (42,56,57), which could possibly reflect age-related reduction in neuronal activity.

Admittedly, our study was susceptible to several technical limitations that could also lead to an appearance of heterogeneity. For example, since the anterior hippocampus is thicker and has more folds than the posterior hippocampus, progressive partial volume may develop along its length (Fig 1b). Furthermore, since the anterior hippocampus is closer to the skull base, field inhomogeneity caused by nearby

bone-air-tissue interfaces, chiasmal fat, or clival marrow is more likely to distort spectra (48,58,59). Given the small voxel size in this study, however, random variation in their cerebrospinal fluid partial volume is an unlikely cause of these linear metabolic gradients. If it were, then the slopes of all the metabolites within any individual should have been the same, given that cerebrospinal fluid partial volume reduces all metabolic content in a voxel, equally.

In addition, voxels in the posterior region might have also included parahippocampal white matter and possibly thalamus. Once again, we believe that small voxel size prevented substantial bias in voxel composition. Indeed, since the observed gradients are significantly different among the three metabolites, as shown in Figure 4, the gradients are unlikely to reflect partial volume. For the same reason, these gradients are also unlikely to reflect B_1 inhomogeneity in the VOI, minor as it may be. Finally, since the anterior hippocampus is thicker than the posterior hippocampus (Fig 1), less partial volume is expected there, suggesting that if that is the underlying cause of the differences in the gradients, they would be in the opposite direction from what was observed.

Furthermore, the standard errors of the means in Figure 4 (ie, 12.5%, 18%, and 20% for NAA, creatine, and choline, respectively) translate, when corrected for sample size $(n = 6)^{1/2}$ per age group, to 25%, 36%, and 40%, respectively, in any voxel. The corrected values are not much different from the predicted intraindividual reproducible values for cerebrospinal fluid–free voxels of this size (60). These two observations combine to support the notion that metabolic heterogeneity is unlikely to be an artifact of either the measurement technique or postprocessing.

In conclusion, this study affirms that, even in healthy young adults, the hippocampus exhibits regional metabolic heterogeneity detectable with the sensitivity of ^{1}H MR spectroscopy at 3 T. Anteroposterior axis metabolic gradients are clearly seen, and this observation may reflect the division of function within this structure. Consequently, with the use of ^{1}H MR spectroscopy in the hippocampus, clinicians should strive for consistent voxel placement to ensure that the same region is compared for either absolute quantification or for metabolite ratios from different studies or at different times. Results of this study indicate that not all regions in the hippocampus can be treated as metabolically equivalent.

In sum, our major findings are that there is a heterogeneous distribution of metabolites within the hippocampus and that, in general, there is a higher concentration of metabolites posteriorly than anteriorly; also, we found that concentrations are higher in the young than in the elderly everywhere along the hippocampus.

Acknowledgments: The authors thank Roman Fleysher, PhD, and Lazar Fleysher, PhD, New York University, New York, for their help in determining the T1 and T2 values of the metabolites in the reference phantom and Andrew A. Maudsley, PhD, University of Miami, Miami, Fla, and Brian J. Soher, PhD, Duke University, Durham, NC, for the use of their SITools-FITT spectral modeling software.

References

1. de Leon M, Bobinski M, Convit A, De Santi S. Neuropathological and neuroimaging studies of the hippocampus in normal aging and in Alzheimer's disease. New York, NY: Oxford University Press, 1999.
2. Sweatt JD. Hippocampal function in cognition. Psychopharmacology 2004;174:99–110.
3. Campbell S, Macqueen G. The role of the hippocampus in the pathophysiology of major depression. J Psychiatry Neurosci 2004; 29:417–426.
4. Bremner J. Brain pathways in stress processing. Biol Psychiatry 2002;51:91S–92S.
5. Notle J. The human brain: an introduction to its functional anatomy. St Louis, Mo: Mosby, 1999.
6. Cendes F. Progressive hippocampal and extrahippocampal atrophy in drug resistant epilepsy. Curr Opin Neurol 2005;18:173–177.
7. Heckers S, Konradi C. Hippocampal neurons in schizophrenia. J Neural Transm 2002;109:891–905.
8. Sala M, Perez J, Soloff P, et al. Stress and hippocampal abnormalities in psychiatric disorders. Eur Neuropsychopharmacol 2004;14:393–405.
9. Kantarci K, Jack CR Jr. Neuroimaging in Alzheimer disease: an evidence-based review. Neuroimaging Clin N Am 2003;13: 197–209.
10. Simmons ML, Frondoza CG, Coyle JT. Immunocytochemical localization of N-acetylaspartate with monoclonal antibodies. Neuroscience 1991;45:37–45.
11. Miller BL. A review of chemical issues in 1H NMR spectroscopy: N-acetyl-L-aspartate, creatine and choline. NMR Biomed 1991;4: 47–52.
12. McIlwain H, Bachelard HS. Biochemistry and the central nervous system. Edinburgh, Scotland: Churchill Livingstone, 1985.
13. Posse S, Schuknecht B, Smith ME, van Zijl PC, Herschkowitz N, Moonen CT. Short echo time proton MR spectroscopic imaging. J Comput Assist Tomogr 1993;17:1–14.
14. Gonen O, Arias-Mendoza F, Goelman G. 3D localized in vivo 1H spectroscopy of human brain by using a hybrid of 1D-Hadamard with 2D-chemical shift imaging. Magn Reson Med 1997;37:644–650.
15. Lichy MP, Bachert P, Hamprecht F, et al. Application of (1)H MR spectroscopic imaging in radiation oncology: choline as a marker for determining the relative probability of tumor progression after radiation of glial brain tumors [in German]. Rofo 2006; 178:627–633.
16. Stadlbauer A, Gruber S, Nimsky C, et al. Preoperative grading of gliomas by using metabolite quantification with high-spatial-resolution proton MR spectroscopic imaging. Radiology 2006;238:958–969.
17. Mueller SG, Laxer KD, Suhy J, Lopez RC, Flenniken DL, Weiner MW. Spectroscopic metabolic abnormalities in mTLE with and without MRI evidence for mesial temporal sclerosis using hippocampal short-TE MRSI. Epilepsia 2003;44:977–980.
18. Soher BJ, Doraiswamy PM, Charles HC. A review of 1H MR spectroscopy findings in Alzheimer's disease. Neuroimaging Clin N Am 2005;15:847–852, xi.
19. Kuzniecky R, Hugg JW, Hetherington H, et al. Relative utility of 1H spectroscopic imaging and hippocampal volumetry in the lateralization of mesial temporal lobe epilepsy. Neurology 1998;51:66–71.
20. Mueller SG, Laxer KD, Barakos JA, et al. Identification of the epileptogenic lobe in neocortical epilepsy with proton MR spectroscopic imaging. Epilepsia 2004;45:1580–1589.
21. Dam AM. Epilepsy and neuron loss in the hippocampus. Epilepsia 1980;21:617–629.
22. Mouritzen Dam A. The density of neurons in

the human hippocampus. Neuropathol Appl Neurobiol 1979;5:249–264.

23. Vermathen P, Laxer KD, Matson GB, Weiner MW. Hippocampal structures: anteroposterior N-acetylaspartate differences in patients with epilepsy and control subjects as shown with proton MR spectroscopic imaging. Radiology 2000;214:403–410.

24. Hetherington HP, Kim JH, Pan JW, Spencer DD. 1H and 31P spectroscopic imaging of epilepsy: spectroscopic and histologic correlations. Epilepsia 2004;45(suppl 4):17–23.

25. Folstein MF, Robins LN, Helzer JE. The Mini-Mental State Examination. Arch Gen Psychiatry 1983;40:812.

26. Reisberg B, Ferris SH, de Leon MJ, Crook T. Global Deterioration Scale (GDS). Psychopharmacol Bull 1988;24:661–663.

27. Reisberg B, Ferris SH. Brief Cognitive Rating Scale (BCRS). Psychopharmacol Bull 1988; 24:629–636.

28. Hu J, Javaid T, Arias-Mendoza F, Liu Z, McNamara R, Brown TR. A fast, reliable, automatic shimming procedure using 1H chemical-shift-imaging spectroscopy. J Magn Reson B 1995;108:213–219.

29. Goelman G, Liu S, Hess D, Gonen O. Optimizing the efficiency of high-field multivoxel spectroscopic imaging by multiplexing in space and time. Magn Reson Med 2006;56: 34–40.

30. Mareci T, Brooker H. Essential considerations for spectral localization using indirect gradient encoding of spatial information. J Magn Reson 1991;92:229–246.

31. Goelman G, Liu S, Gonen O. Reducing voxel bleed in Hadamard-encoded MRI and MRS. Magn Reson Med 2006;55:1460–1465.

32. Brown TR. Practical applications of chemical shift imaging. NMR Biomed 1992;5:238–243.

33. De Santi S, de Leon MJ, Rusinek H, et al. Hippocampal formation glucose metabolism and volume losses in MCI and AD. Neurobiol Aging 2001;22:529–539.

34. Soher BJ, Young K, Govindaraju V, Maudsley AA. Automated spectral analysis. III. Application to in vivo proton MR spectroscopy and spectroscopic imaging. Magn Reson Med 1998;40:822–831.

35. Soher BJ, Young K, Maudsley AA. Representation of strong baseline contributions in 1H MR spectra. Magn Reson Med 2001;45:966–972.

36. Inglese M, Li BS, Rusinek H, Babb JS, Grossman RI, Gonen O. Diffusely elevated cerebral choline and creatine in relapsing-remitting multiple sclerosis. Magn Reson Med 2003;50:190–195.

37. Zaaraoui W, Fleysher L, Fleysher R, Liu S, Soher BJ, Gonen O. Human brain-structure resolved T(2) relaxation times of proton metabolites at 3 Tesla. Magn Reson Med 2007; 57:983–989.

38. Barker PB, Soher BJ, Blackband SJ, Chatham JC, Mathews VP, Bryan RN. Quantitation of proton NMR spectra of the human brain using tissue water as an internal concentration reference. NMR Biomed 1993;6: 89–94.

39. Mlynarik V, Gruber S, Moser E. Proton T (1) and T (2) relaxation times of human brain metabolites at 3 Tesla. NMR Biomed 2001; 14:325–331.

40. Fleysher L, Fleysher R, Liu S, Zaaraoui W, Gonen O. Optimizing the precision-per-unit-time of quantitative MR metrics: examples for T1, T2, and DTI. Magn Reson Med 2007; 57:380–387.

41. Fleysher R, Fleysher L, Gonen O. The optimal MR acquisition strategy for exponential decay constants estimation. Magn Reson Imaging 2008;26:433–435.

42. Schuff N, Amend DL, Knowlton R, Norman D, Fein G, Weiner MW. Age-related metabolite changes and volume loss in the hippocampus by magnetic resonance spectroscopy and imaging. Neurobiol Aging 1999;20: 279–285.

43. Brooks JC, Roberts N, Kemp GJ, Gosney MA, Lye M, Whitehouse GH. A proton magnetic resonance spectroscopy study of age-related changes in frontal lobe metabolite concentrations. Cereb Cortex 2001;11:598–605.

44. Angelie E, Bonmartin A, Boudraa A, Gonnaud PM, Mallet JJ, Sappey-Marinier D. Regional differences and metabolic changes in normal aging of the human brain: proton MR spectroscopic imaging study. AJNR Am J Neuroradiol 2001;22: 119–127.

45. Charles HC, Lazeyras F, Krishnan KR, et al. Proton spectroscopy of human brain: effects of age and sex. Prog Neuropsychopharmacol Biol Psychiatry 1994;18:995–1004.

46. Colombo M, Fernandez T, Nakamura K, Gross CG. Functional differentiation along the anterior-posterior axis of the hippocampus in monkeys. J Neurophysiol 1998;80: 1002–1005.

47. Paller KA, McCarthy G. Field potentials in the human hippocampus during the encoding and recognition of visual stimuli. Hippocampus 2002;12:415–420.

48. Greicius MD, Krasnow B, Boyett-Anderson JM, et al. Regional analysis of hippocampal activation during memory encoding and retrieval: fMRI study. Hippocampus 2003; 13:164–174.

49. Canteras NS, Swanson LW. Projections of the ventral subiculum to the amygdala, septum, and hypothalamus: a PHAL anterograde tract-tracing study in the rat. J Comp Neurol 1992;324:180–194.

50. Moser MB, Moser EI. Functional differentiation in the hippocampus. Hippocampus 1998;8:608–619.

51. Isaacson RL, Pribram KH. The hippocampus. New York, NY: Plenum, 1975.

52. Saunders DE, Howe FA, van den Boogaart A, Griffiths JR, Brown MM. Aging of the adult human brain: in vivo quantitation of metabolite content with proton magnetic resonance spectroscopy. J Magn Reson Imaging 1999;9:711–716.

53. Chang L, Ernst T, Poland RE, Jenden DJ. In vivo proton magnetic resonance spectroscopy of the normal aging human brain. Life Sci 1996;58:2049–2056.

54. Harada M, Miyoshi H, Otsuka H, Nishitani H, Uno M. Multivariate analysis of regional metabolic differences in normal ageing on localised quantitative proton MR spectroscopy. Neuroradiology 2001;43:448–452.

55. Chen JG, Charles HC, Barboriak DP, Doraiswamy PM. Magnetic resonance spectroscopy in Alzheimer's disease: focus on N-acetylaspartate. Acta Neurol Scand Suppl 2000;176:20–26.

56. Szentkuti A, Guderian S, Schiltz K, et al. Quantitative MR analyses of the hippocampus: unspecific metabolic changes in aging. J Neurol 2004; 251:1345–1353.

57. Driscoll I, Hamilton DA, Petropoulos H, et al. The aging hippocampus: cognitive, biochemical and structural findings. Cereb Cortex 2003;13:1344–1351.

58. Schuff N, Amend D, Ezekiel F, et al. Changes of hippocampal N-acetyl aspartate and volume in Alzheimer's disease: a proton MR spectroscopic imaging and MRI study. Neurology 1997;49:1513–1521.

59. Parmar H, Lim TC, Yin H, et al. Multi-voxel MR spectroscopic imaging of the brain: utility in clinical setting—initial results. Eur J Radiol 2005;55:401–408.

60. Li BS, Babb JS, Soher BJ, Maudsley AA, Gonen O. Reproducibility of 3D proton spectroscopy in the human brain. Magn Reson Med 2002;47:439–446.

Radiology 2008

This is your reprint order form or pro forma invoice

(Please keep a copy of this document for your records.)

Reprint order forms and purchase orders or prepayments must be received 72 hours after receipt of form either by mail or by fax at 410-820-9765. It is the policy of Cadmus Reprints to issue one invoice per order. **Please print clearly**.

Author Name _____
Title of Article _____
Issue of Journal_____ Reprint # _____ Publication Date _____
Number of Pages_____ KB # _____ Symbol Radiology
Color in Article? Yes / No (Please Circle)

Please include the journal name and reprint number or manuscript number on your purchase order or other correspondence.

Order and Shipping Information

Reprint Costs **(Please see page 2 of 2 for reprint costs/fees.)**

_____ Number of reprints ordered $_____
_____ Number of color reprints ordered $_____
_____ Number of covers ordered $_____
Subtotal $_____
Taxes $_____

(*Add appropriate sales tax for Virginia, Maryland, Pennsylvania, and the District of Columbia or Canadian GST to the reprints if your order is to be shipped to these locations*.)

First address included, add $32 for each additional shipping address $_____

TOTAL $_____

Shipping Address **(cannot ship to a P.O. Box) Please Print Clearly**

Name _____
Institution _____
Street _____
City _____ State _____ Zip _____
Country _____
Quantity_____ Fax _____
Phone: Day _____ Evening _____
E-mail Address _____

Additional Shipping Address* **(cannot ship to a P.O. Box)**

Name _____
Institution _____
Street _____
City _____ State _____ Zip _____
Country _____
Quantity _____ Fax _____
Phone: Day _____ Evening _____
E-mail Address _____
** Add $32 for each additional shipping address*

Payment and Credit Card Details

Enclosed: Personal Check _____
Credit Card Payment Details _____
Checks must be paid in U.S. dollars and drawn on a U.S. Bank.

Credit Card: __ VISA __ Am. Exp. __ MasterCard
Card Number _____
Expiration Date_____
Signature: _____

Please send your order form and prepayment made payable to:

Cadmus Reprints
P.O. Box 751903
Charlotte, NC 28275-1903

Note: Do not send express packages to this location, PO Box.
FEIN #:541274108

Invoice or Credit Card Information

Invoice Address Please Print Clearly
Please complete Invoice address as it appears on credit card statement

Name _____
Institution _____
Department _____
Street _____
City _____ State _____ Zip _____
Country _____
Phone _____ Fax _____
E-mail Address _____

Cadmus will process credit cards and *Cadmus Journal Services* will appear on the credit card statement.

If you don't mail your order form, you may fax it to 410-820-9765 with your credit card information.

Signature _____ Date _____
Signature is required. By signing this form, the author agrees to accept the responsibility for the payment of reprints and/or all charges described in this document.

RB-9/26/07

Radiology 2008

Black and White Reprint Prices

Domestic (USA only)						
# of Pages	50	100	200	300	400	500
1-4	$221	$233	$268	$285	$303	$323
5-8	$355	$382	$432	$466	$510	$544
9-12	$466	$513	$595	$652	$714	$775
13-16	$576	$640	$749	$830	$912	$995
17-20	$694	$775	$906	$1,017	$1,117	$1,220
21-24	$809	$906	$1,071	$1,200	$1,321	$1,471
25-28	$928	$1,041	$1,242	$1,390	$1,544	$1,688
29-32	$1,042	$1,178	$1,403	$1,568	$1,751	$1,924
Covers	$97	$118	$215	$323	$442	$555

International (includes Canada and Mexico)						
# of Pages	50	100	200	300	400	500
1-4	$272	$283	$340	$397	$446	$506
5-8	$428	$455	$576	$675	$784	$884
9-12	$580	$626	$805	$964	$1,115	$1,278
13-16	$724	$786	$1,023	$1,232	$1,445	$1,652
17-20	$878	$958	$1,246	$1,520	$1,774	$2,030
21-24	$1,022	$1,119	$1,474	$1,795	$2,108	$2,426
25-28	$1,176	$1,291	$1,700	$2,070	$2,450	$2,813
29-32	$1,316	$1,452	$1,936	$2,355	$2,784	$3,209
Covers	$156	$176	$335	$525	$716	$905

Color Reprint Prices

Domestic (USA only)						
# of Pages	50	100	200	300	400	500
1-4	$223	$239	$352	$473	$597	$719
5-8	$349	$401	$601	$849	$1,099	$1,349
9-12	$486	$517	$852	$1,232	$1,609	$1,992
13-16	$615	$651	$1,105	$1,609	$2,117	$2,624
17-20	$759	$787	$1,357	$1,997	$2,626	$3,260
21-24	$897	$924	$1,611	$2,376	$3,135	$3,905
25-28	$1,033	$1,071	$1,873	$2,757	$3,650	$4,536
29-32	$1,175	$1,208	$2,122	$3,138	$4,162	$5,180
Covers	$97	$118	$215	$323	$442	$555

International (includes Canada and Mexico))						
# of Pages	50	100	200	300	400	500
1-4	$278	$290	$424	$586	$741	$904
5-8	$429	$472	$746	$1,058	$1,374	$1,690
9-12	$604	$629	$1,061	$1,545	$2,011	$2,494
13-16	$766	$797	$1,378	$2,013	$2,647	$3,280
17-20	$945	$972	$1,698	$2,499	$3,282	$4,069
21-24	$1,110	$1,139	$2,015	$2,970	$3,921	$4,873
25-28	$1,290	$1,321	$2,333	$3,437	$4,556	$5,661
29-32	$1,455	$1,482	$2,652	$3,924	$5,193	$6,462
Covers	$156	$176	$335	$525	$716	$905

Minimum order is 50 copies. For orders larger than 500 copies, please consult Cadmus Reprints at 800-407-9190.

Reprint Cover

Cover prices are listed above. The cover will include the publication title, article title, and author name in black.

Shipping

Shipping costs are included in the reprint prices. Domestic orders are shipped via UPS Ground service. Foreign orders are shipped via a proof of delivery air service.

Multiple Shipments

Orders can be shipped to more than one location. Please be aware that it will cost $32 for each additional location.

Delivery

Your order will be shipped within 2 weeks of the journal print date. Allow extra time for delivery.

Tax Due

Residents of Virginia, Maryland, Pennsylvania, and the District of Columbia are required to add the appropriate sales tax to each reprint order. For orders shipped to Canada, please add 7% Canadian GST unless exemption is claimed.

Ordering

Reprint order forms and purchase order or prepayment is required to process your order. Please reference journal name and reprint number or manuscript number on any correspondence. You may use the reverse side of this form as a proforma invoice. Please return your order form and prepayment to:

Cadmus Reprints
P.O. Box 751903
Charlotte, NC 28275-1903

Note: Do not send express packages to this location, PO Box.
FEIN #:541274108

Please direct all inquiries to:

Rose A. Baynard
800-407-9190 (toll free number)
410-819-3966 (direct number)
410-820-9765 (FAX number)
baynardr@cadmus.com (e-mail)

Reprint Order Forms and purchase order or prepayments must be received 72 hours after receipt of form.